J. Fluid Mech. (1993), *vol.* 254, *pp.* 401–416

The evolution of thermocline waves from an oscillatory disturbance

By D. NICOLAOU†, R. LIU AND T. N. STEVENSON
Department of Engineering, University of Manchester, Oxford Road, Manchester M13 9PL, UK

(Received 11 January 1992 and in revised form 25 February 1993)

The way in which energy propagates away from a two-dimensional oscillatory disturbance in a thermocline is considered theoretically and experimentally. It is shown how the St. Andrew's-cross-wave is modified by reflections and how the cross-wave can develop into thermocline waves. A linear shear flow is then superimposed on the thermocline. Ray theory is used to evaluate the wave shapes and these are compared to finite-difference solutions of the full Navier–Stokes equations.

1. Introduction

A horizontal cylinder, oscillating with frequency ω in a density-stratified fluid with a background natural frequency N, will produce a St. Andrew's-cross-wave with the four arms, or beams of energy, inclined at angles of $\theta = \mp \sin(\omega/N)$ to the horizontal (see the reviews by Roberts 1975 and Lighthill 1978). The ray paths along which the energy propagates are coincident with the lines of constant phase. Point disturbance theory predicts an infinitesimally thin beam in each direction, whereas in experiments the beams have a finite width over which the phase varies. If the point disturbance had been moving with a mean velocity relative to the fluid, all wavenumbers would be uniquely determined by a Doppler relation and the wave spacing over the whole of the far field would be known even from the inviscid point disturbance theory (see Stevenson 1973). The width of the beams from an oscillatory disturbance can be determined theoretically by satisfying the boundary conditions around a finite-sized body (see for example Appleby & Crighton 1986; Voisin 1991). Viscosity produces the increase in width of the beams with distance from the source that is observed experimentally (see Thomas & Stevenson 1972 and Gordon, Klement & Stevenson 1975). A linear viscous analysis (Makarov, Neklyudov & Chashechkin 1990) shows how the amplitude distribution in the beams depends on the size of the body; larger bodies produce twin-peaked distributions. Kistovich, Neklyudov & Chashechkin (1990) show how nonlinear effects can produce several harmonics which propagate in the directions given by linear theory for the fundamental frequency.

When the natural frequency N varies with height the beams from an oscillatory disturbance are curved and reflections occur at a level where $N = \omega$ (see Phillips 1966). The present paper uses ray theory, finite-difference calculations and experiments to show the way in which the beams, after several reflections within a thermocline, eventually produce the 'thermocline waves' of the type described by Krauss (1966) and Thorpe (1968). The effects of a shear flow, in which the background velocity varies linearly with height, are then included and it is shown that there is less tendency to produce thermocline waves. The finite-difference method used to solve the full

† Present address: Department of Mechanical Engineering, University of Liverpool, PO Box 147, Liverpool, L69 3BX, UK.

Navier–Stokes equations is based on the 'marker and cell' method of Harlow & Welch (1965) and Young & Hirt (1972). The method was extended to a moving body in a stratified fluid by Nicolaou (1987) and open boundaries were included by Liu & Stevenson (1989). The program was used to study a cross-wave in a shear flow with constant N (Liu, Nicolaou & Stevenson 1990).

2. Ray paths and the phase configuration

A coordinate system $[x, z]$ is defined with the origin on the thermocline centreline and with x and z positive to the right and vertically upwards respectively. The mean position of the oscillatory disturbance is at $[0, z_1]$. The background stratified fluid is stable with a natural frequency distribution $N(z)$ and with a background horizontal flow $U(z)$. Ray theory for this problem was given by Liu *et al.* (1990) and is based on that of Stevenson (1973). Under the WKB approximation the propagation of energy at a point is described by the group velocity equations which apply to a uniform stratified flow with a constant natural frequency. The energy moves on ray paths along which the horizontal wavenumber component k and the frequency ω are constant. The frequency relation (Bretherton 1966) is

$$\omega = \omega_r(z) + kU(z), \tag{1}$$

where ω_r is the frequency relative to the fluid and ω is the oscillatory frequency of the source. U must be zero at the level of the source otherwise a steady lee wave system will be superimposed on the oscillatory waves.

The dispersion relation is

$$\omega_r^2 = \frac{[N(z)]^2 k^2}{k^2 + [m(z)]^2} = [N(z)]^2 \sin^2\theta(z), \tag{2}$$

where the wavenumber is $\boldsymbol{k} = [k, m]$ and $\theta(z)$ is the angle that the ray path makes with the horizontal in a frame of reference moving with the background flow at that level. $\theta(z)$ is measured anticlockwise from the positive x-direction. The ray paths are defined by

$$\frac{\mathrm{d}x}{\mathrm{d}t} = U + u_{gr} \quad \text{and} \quad \frac{\mathrm{d}z}{\mathrm{d}t} = w_{gr}, \tag{3}$$

where $[u_{gr}, w_{gr}]$ is the group velocity relative to the background fluid. The relation $k = -m\tan\theta$ satisfies the condition that the phase velocity is directed towards the horizontal level from which the energy is propagating. From this relation and (2) the group velocity $(\partial\omega_r/\partial k, \partial\omega_r/\partial m]$ is given by

$$[u_{gr}, w_{gr}] = \omega_r k^{-1} \sin\theta\cos\theta[\cot\theta, 1]. \tag{4}$$

The direction in which energy propagates along a ray path is determined from the radiation condition which implies that $\mathrm{d}t > 0$. From (3) and (4), noting that $\mathrm{d}z$ and $\sin\theta$ have the same sign, the condition is $k/(\omega_r\cos\theta) > 0$. At the position of the source where $U = 0$ the energy begins to propagate along the four beams. At time t the phase of the energy which left the disturbance at time t_1 is

$$\phi = -\omega t_1 + \int_{t_1}^{t} (kU - \omega)\,\mathrm{d}t + \phi_R = -\omega t + F + \phi_R, \tag{5}$$

where, from (3),

$$F = k\int_{z_1}^{z} \frac{U}{w_{gr}}\,\mathrm{d}z. \tag{6}$$

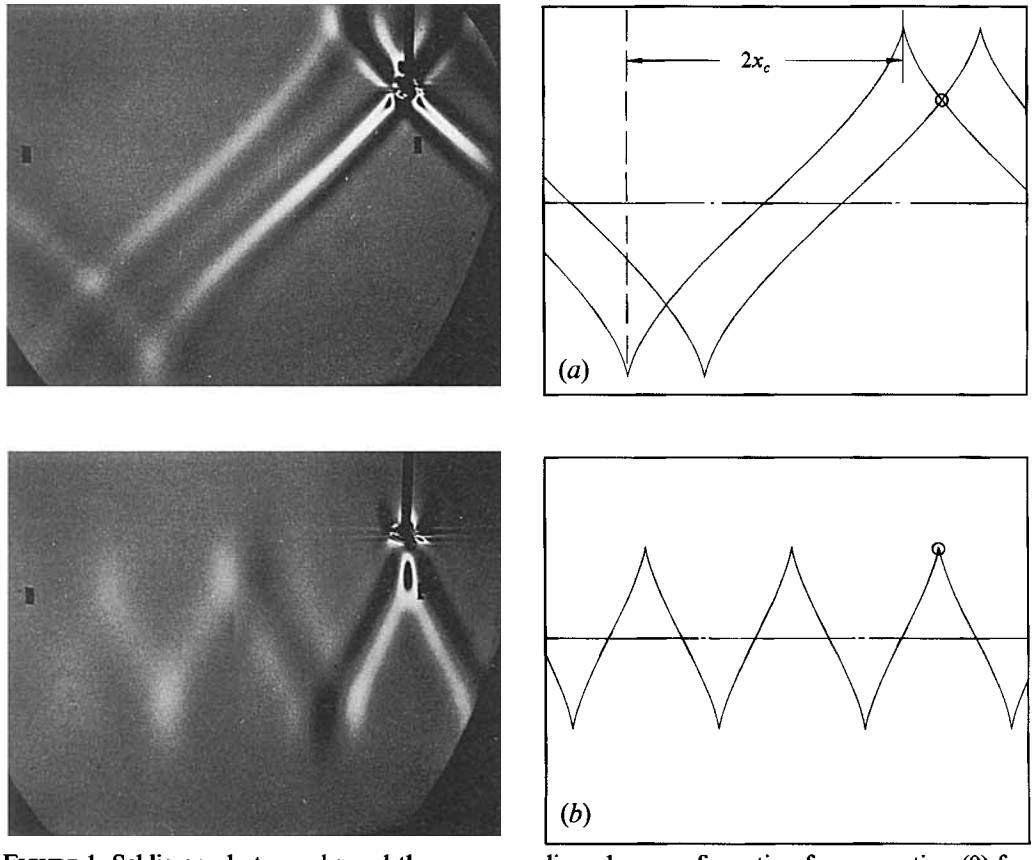

FIGURE 1. Schlieren photographs and the corresponding phase configuration from equation (9) for a horizontal cylinder oscillating with (*a*) $\Omega = 0.69$ and (*b*) 0.91 in a thermocline with no background flow. The width of each picture is 390 mm, $\epsilon = 325$ mm and $N_c = 1.02$ rad/s. The black vertical line at the top of the photographs is the cylinder support.

In (5), ωt_1 is the phase of the source at time t_1, z_1 is the vertical position of the source and ϕ_R is the sum of the phase shifts which occur at the caustics. The lines of constant phase may be evaluated from (5) and (6) together with an equation for the ray paths derived from (3), (4) and (6),

$$x = \int_{z_1}^{z} \cot\theta \, \mathrm{d}z + \frac{F}{k}. \tag{7}$$

Ray theory cannot strictly be taken to the caustic where $\omega_r = N(z)$ but, as was shown by Lighthill (1978) for a uniform flow and by Liu (1989) for a sheared flow, ray theory can be matched to an Airy function which 'heals' the solution. The phase shift in time as the wave reflects is a $\frac{1}{2}\pi$ lag in the vertical velocity component and a $\frac{1}{2}\pi$ lead in the horizontal velocity component.

3. Waves in a thermocline

From (2), (6) and (7) when $U = 0$ the ray paths are given by

$$x = \int_{z_1}^{z} \left\{ \frac{[N(z)]^2}{\omega^2} - 1 \right\}^{\frac{1}{2}} \mathrm{d}z. \tag{8}$$

A hyperbolic tangent density profile (Groen 1948) with its corresponding natural

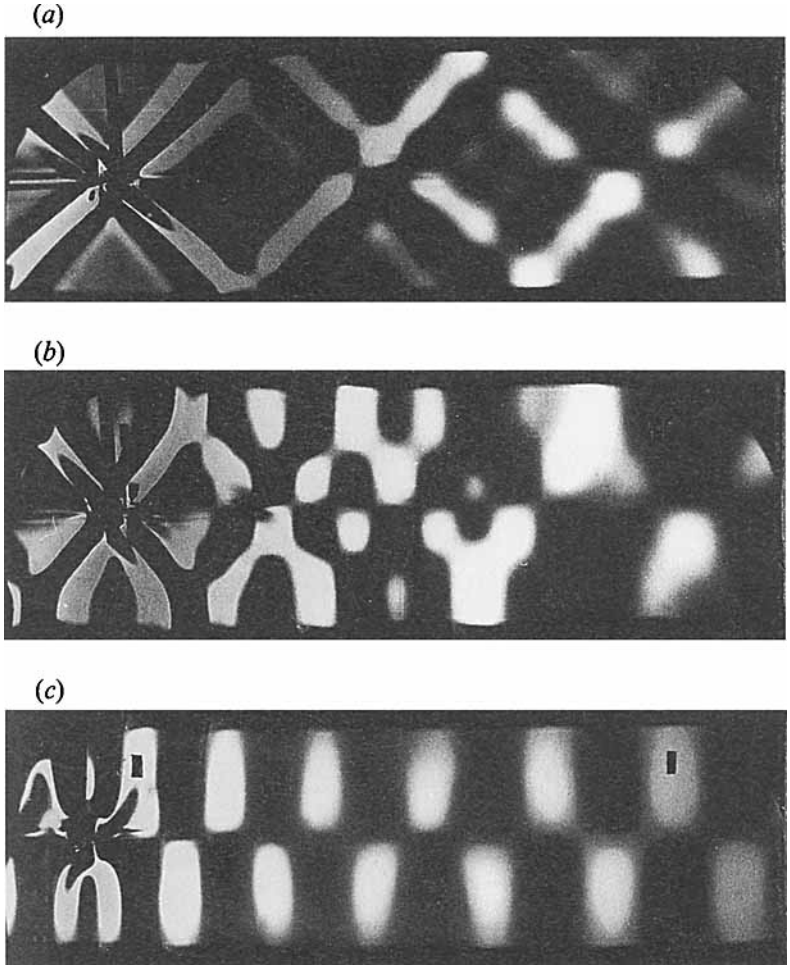

FIGURE 2. Schlieren photographs showing the development of thermocline waves from St. Andrew's-cross-waves when there is no background flow. The cylinder is oscillating in a horizontal plane which produces odd-mode thermocline waves. $N_c = 1.34$ rad/s, $\epsilon = 188$ mm and Ω for (*a*) is 0.62, (*b*) 0.75 and (*c*) 0.88. A strong $n = 1$ mode is shown in (*c*). The width of the pictures is 450 mm.

frequency distribution $N(z) = N_c \operatorname{sech}(2z/\epsilon)$, is often used to represent a thermocline. N_c is the natural frequency at the centre of the thermocline and ϵ is a thermocline thickness. With this distribution the ray path and the phase configuration are given by

$$X = G(Z) - G(Z_1), \tag{9}$$

where

$$G(Z) = \Omega^{-1} \tan^{-1}\left\{\frac{\sinh Z}{(1-\Omega^2\cosh^2 Z)^{\frac{1}{2}}}\right\} - \sin^{-1}\left\{\frac{\Omega \sinh Z}{(1-\Omega^2)^{\frac{1}{2}}}\right\}. \tag{10}$$

$X = 2x/\epsilon$, $Z = 2z/\epsilon$, $Z_1 = 2z_1/\epsilon$ and $\Omega = \omega/N_c$.

In figure 1 the phase configurations from this equation are compared with schlieren photographs showing wave beams from an oscillating cylinder which is above the centreline of a thermocline. If the horizontal distance between consecutive upper and lower caustics on a ray is $2x_c$ (see figure 1) then from (10)

$$X_c = 2x_c/\epsilon = G(Z_U) - G(Z_L) = \pi(\Omega^{-1} - 1), \tag{11}$$

where the subscripts U and L refer to the upper and lower caustics. All the photographs

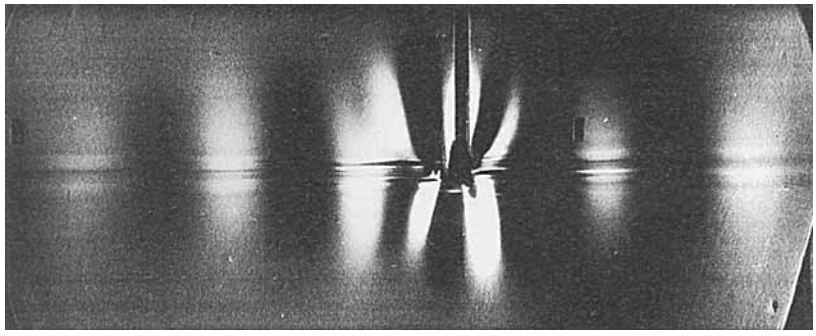

FIGURE 3. The cylinder is oscillating in a vertical plane and an $n = 0$ thermocline mode is produced. $N_c = 0.76$ rad/s, $\epsilon = 170$ mm and $\Omega = 0.92$. There is no background flow. The width of the picture is 450 mm.

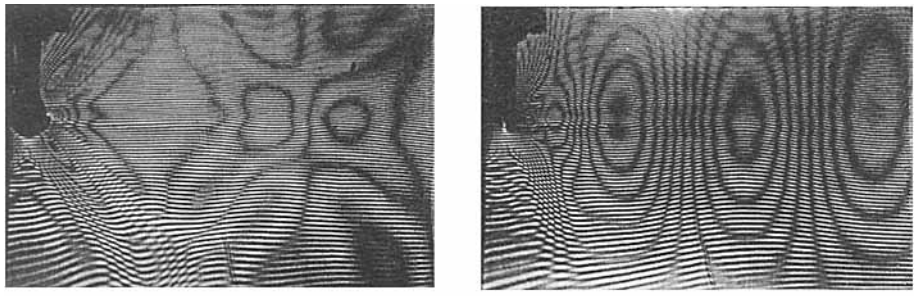

(*a*) (*b*)

FIGURE 4. Composite interferograms showing the waves from a vertically oscillating cylinder producing even thermocline modes with no background flow. $N_c = 1.62$ rad/s, $\epsilon = 140$ mm and Ω for (*a*) is 0.8 and for (*b*) 0.95. The width of the pictures is 95 mm.

in this paper are taken through the glass sides of a tank of stratified brine, looking along the axis of a horizontal cylinder which is supported on a strut from the top of the tank. The thermocline in the tank was produced by allowing an interface between water and brine to diffuse; the diffusion profile is close to a hyperbolic tangent profile (Stevenson, Kanellopulos & Constantinides 1986). In figure 1(*b*), ω is equal to $N(z_1)$ at the level of the cylinder so that wave energy cannot propagate above the cylinder. The beams bend towards the vertical as the waves propagate into regions of lower $N(z)$, reflect at the upper and lower caustics where $N(z) = \omega$ and generally propagate horizontally with the thermocline acting as a wave guide. The ray paths which are also isophase lines have a point of inflexion at the centre of the thermocline and along each ray there is a $\frac{1}{2}\pi$ phase change after every reflection.

The schlieren photographs in figure 2 show how waves from an oscillating cylinder develop into thermocline waves. The initial width of the arms depends on the size of the body and on the amplitude of oscillation. The waves spread as a result of the effects of viscosity and wave path curvature and eventually, sufficiently far from the body, the energy fills the whole of the thermocline between the caustics; a little energy does penetrate into the regions where $N(z) < \omega$ but the velocities fall off exponentially in these regions. As the beams widen to fill the thermocline, there is a transition to thermocline waves. Between the body and the region of thermocline waves there is a complicated web of wave–wave superpositions as an increasing number of widening waves overlap. Thermocline waves develop closer to the body for higher values of Ω or higher ratios of body width to thermocline width.

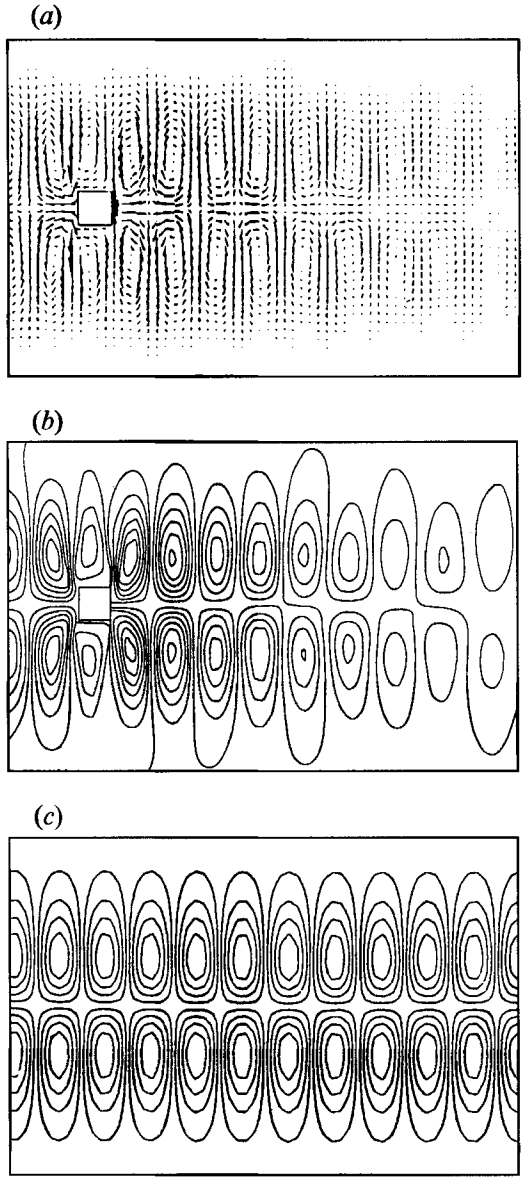

FIGURE 5. (*a*) Velocity vectors, and (*b*, *c*) density perturbation contours: (*a*) and (*b*) are from finite-difference computations and (*c*) is from Thorpe's (1968) solution for an infinite train of waves in an inviscid thermocline. The contour which crosses the centreline in (*b*) has a value very close to zero and its meandering is a result of numerical errors. $N_c = 1.34$ rad/s, $\epsilon = 188$ mm and $\Omega = 0.88$. The height of each diagram is 200 mm. There is no background flow.

Thermocline waves consist of discrete modes which are eigenfunction solutions of the governing equations. The mode number n is the number of vertical-velocity-component sign changes which occur across a vertical section through the thermocline (Lighthill 1978). A cylinder oscillating in a horizontal plane produces odd modes (figure 2) and oscillating in a vertical plane produces even modes as shown by the schlieren photograph in figure 3 and the composite interferograms of figure 4 which show both background fringes and perturbed fringes (see Laws, Peat & Stevenson

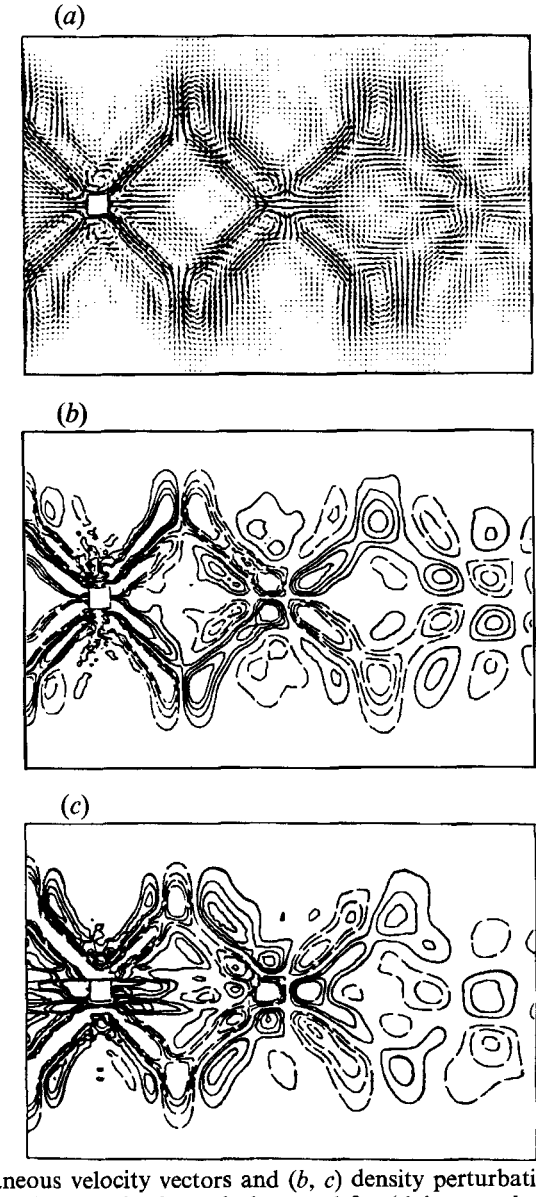

FIGURE 6. (*a*) Instantaneous velocity vectors and (*b*, *c*) density perturbation contours; for (*a*) and (*b*) the cylinder is oscillating in a horizontal plane and for (*c*) in a vertical plane. Finite-difference computations when there is no background flow. $N_c = 1.34$ rad/s, $\epsilon = 188$ mm and $\Omega = 0.6$. The height of each diagram is 320 mm.

1982; Kanellopulos 1982). Figures 3 and 4(*b*) show the beams very quickly disappearing and producing zero-mode thermocline waves which move out horizontally from the source in each direction.

Figures 5(*a*) and 5(*b*) show velocity vector plots and density perturbation contours from the finite-difference program under conditions similar to the photograph of figure 2(*c*). Figure 5(*c*) shows the corresponding inviscid thermocline waves from the theory of Thorpe (1968). There is an error of 12% in the wavelength between the theories and the experiment but this could be a result of a 5% error in ϵ which is within the possible experimental errors. Even though the direction of the vectors cannot be seen in the

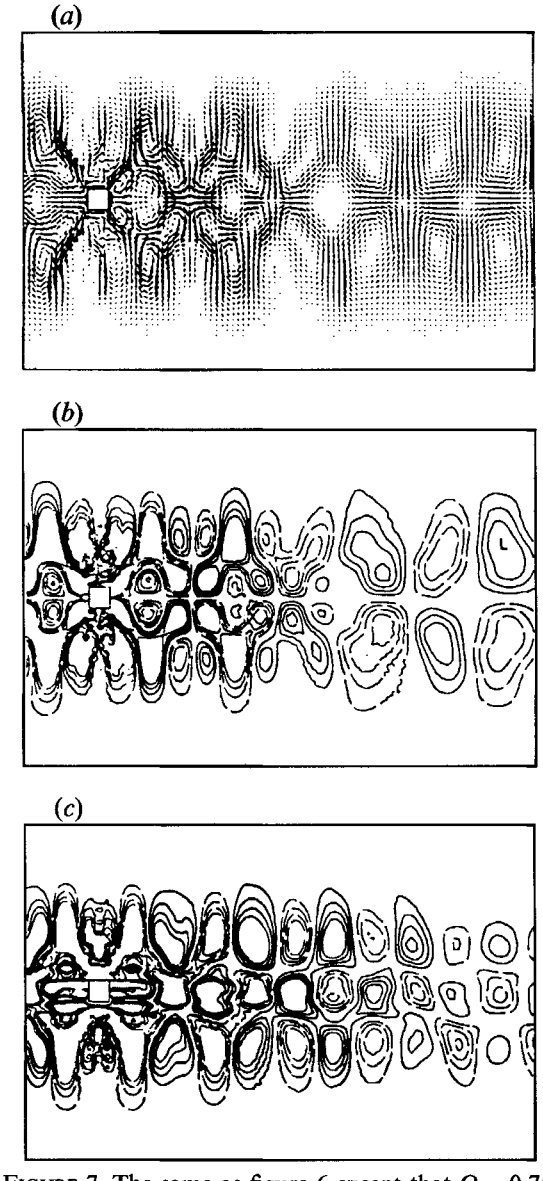

FIGURE 7. The same as figure 6 except that $\Omega = 0.75$.

figure, the lengths do show how the wave strength varies over the field of view. An important feature shown in figures 5(*a*) and 5(*b*) for $\Omega = 0.88$ is the thermocline-type oscillations starting from the body without any individual wave beam structure. The reasons for this will become clearer in the next section. Figures 6 and 7 show that the distance from the source at which thermocline waves appear is greater for lower frequencies. Figures 6(*a*, *b*) and 7(*a*, *b*) show velocity vector plots and density perturbation contours from a body oscillating horizontally under similar conditions to the experiments of figure 2(*a*, *b*). Figures 6(*c*) and 7(*c*) show vertical body oscillations for comparison. For the lower frequency ratio of $\Omega = 0.6$ figure 6(*a*, *b*) shows the trapped wave beams generated near the body developing into a mode $n = 3$ oscillation to the right. For the frequency ratio 0.75, figure 7(*a*, *b*) shows a mode $n = 3$ oscillation

near the body developing into a mode $n = 1$ oscillation further to the right. A vertically oscillating body (figures 6*c* and 7*c*) shows the same process of trapped waves developing through a high-mode thermocline oscillation to a low-mode one but in this case showing even modes.

4. The transition to thermocline modes

The horizontal wavenumber of the thermocline waves can be determined from the trapped wave condition derived by Lighthill (1978),

$$\int_{z_L}^{z_U} m(z)\,\mathrm{d}z = \tfrac{1}{2}\pi(2n+1), \tag{12}$$

where $m(z)$ from the dispersion relation (2) is

$$m(z) = \pm k\left\{\frac{(N(z))^2}{\omega_r^2} - 1\right\}^{\frac{1}{2}}. \tag{13}$$

For the profile $N(z) = N_c \operatorname{sech} Z$, equation (12) becomes

$$(2n+1)\,\pi = K\{G(Z_U) - G(Z_L)\},$$

where $K = k\epsilon$, so that, using (11)

$$K = \frac{(2n+1)\,\Omega}{1-\Omega}. \tag{14}$$

An alternative relationship was derived by Krauss (1966) and Thorpe (1968). The equation for the vertical velocity within a train of thermocline waves together with the boundary conditions that this velocity $\to 0$ as $z \to \pm\,\infty$ yield solutions in terms of hypergeometric functions with the dispersion relation

$$K = \frac{(2n+1)\,\Omega}{1-\Omega^2}\left\{\Omega + \left\{1 - \frac{1-\Omega^2}{(2n+1)^2}\right\}^{\frac{1}{2}}\right\}. \tag{15}$$

This equation reduces to (14) providing $(1-\Omega^2)/(2n+1)^2 \to 0$, which corresponds to large K. It follows that, for a fixed frequency, (14) is a good approximation for the higher-mode thermocline waves. The ray theory and Airy integral formulation which was used to derive (14) is poor for the lowest two modes, $n = 0$ and 1, see Lighthill (1978).

A number of experimental and numerical examples of the transition to thermocline oscillations have been given in the preceding section. This transition is a result of the action of viscosity, wave path curvature and the superposition of waves. A very simple model will enhance the understanding of this transition. We consider the energy leaving the source to the right along the upgoing and downgoing rays. The wave in each ray is assumed to have the form shown in figure 8(*a*) with a wavelength λ and an envelope of width W which increases with distance along the ray as the amplitude decreases. At a fixed time the phase distribution within the envelope remains constant along a ray except after each caustic, where the phase changes by $\frac{1}{2}\pi$. The way in which the waves interact can now be found by summing the waves in all the beams that overlap at any point in the wave field. As an example, when these amplitudes are summed at a fixed height in the thermocline the amplitude distribution looks like that in figure 8(*b*) which shows 'resonant' groups. The wavelength λ_T within the individual groups is constant and equal to that given by (14), with the last group to the right being the lowest mode. It is found that the number of groups between the lowest-mode group and the source

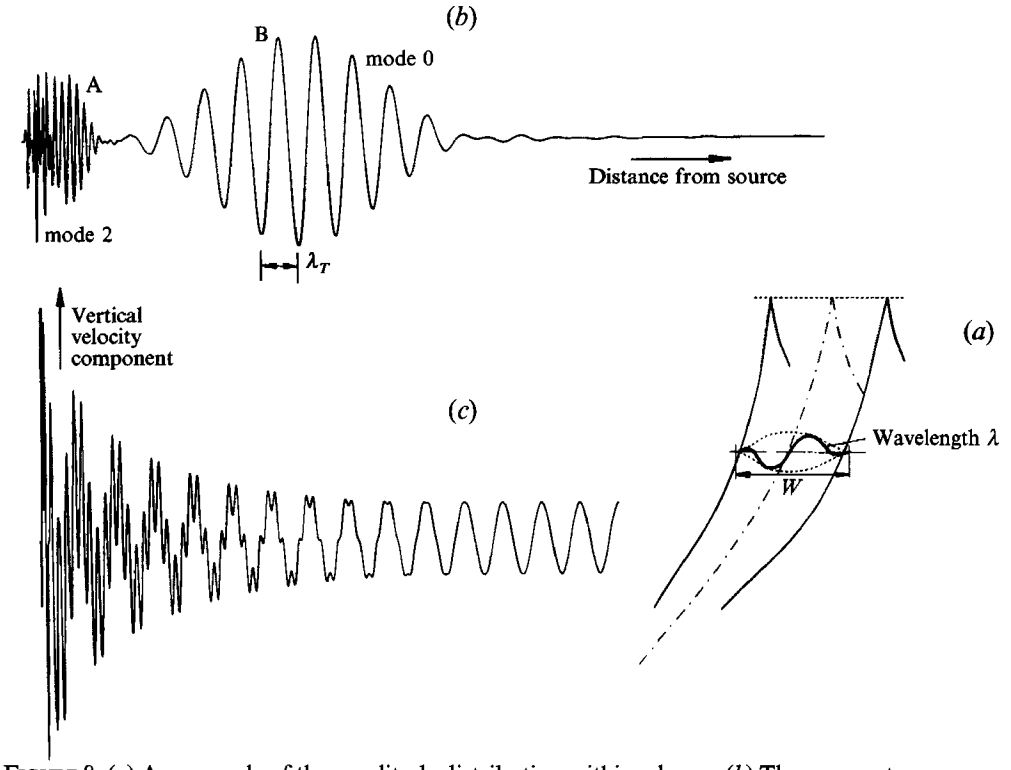

FIGURE 8. (*a*) An example of the amplitude distribution within a beam. (*b*) The resonant wave groups from a superposition of waves at a fixed height in the thermocline. (*c*) As for (*b*) but with a spread rate taken from the viscous similarity solution.

increases as the wavelength λ at the source decreases. Whether even or odd modes develop depends on the initial waveforms leaving the source. If the upgoing and downgoing waveforms are the same then odd modes are produced and if there is a phase difference of π then even modes are produced. Destructive interference results in the small amplitudes between the groups. With R defined as the spread rate $\mathrm{d}W/\mathrm{d}\xi$, where ξ is the distance measured along the ray path from the source, and d is the distance between the thermocline wave groups A and B then, for fixed Ω, the distance d decreases as R increases. For $R = 0$ the original waveform along the rays is repeated every time the rays cross the height level being considered and no thermocline waves develop unless $W \gg 2x_c$, and λ equals a thermocline-mode wavelength.

A small spread rate was used to construct figure 8(*b*) in order to separate the modes. When the width W and the amplitude along the ray path vary as $\xi^{\frac{1}{3}}$ and $\xi^{-\frac{2}{3}}$ respectively, as in the viscous similarity solution of Thomas & Stevenson (1972) then the modes overlap as shown in figure 8(*c*). Changes to the wave width W from curvature effects have not been included. These variations of width and amplitude have also been used to construct figures 9(*a*)–9(*d*) which are similar to figures 2(*a*)–2(*c*) and 4(*b*) respectively. The intensity of the greys in the figures is proportional to density gradient. The good agreement suggests that the mechanisms leading to the transition from a trapped cross-wave to thermocline oscillations have been satisfactorily modelled.

The dimensionless wavelength of thermocline waves, $\Lambda_T = 2\lambda_T/\epsilon$ is, from (14),

$$\Lambda_T = \frac{4\pi}{K} = \frac{4\pi(1-\Omega)}{(2n+1)\,\Omega}.$$

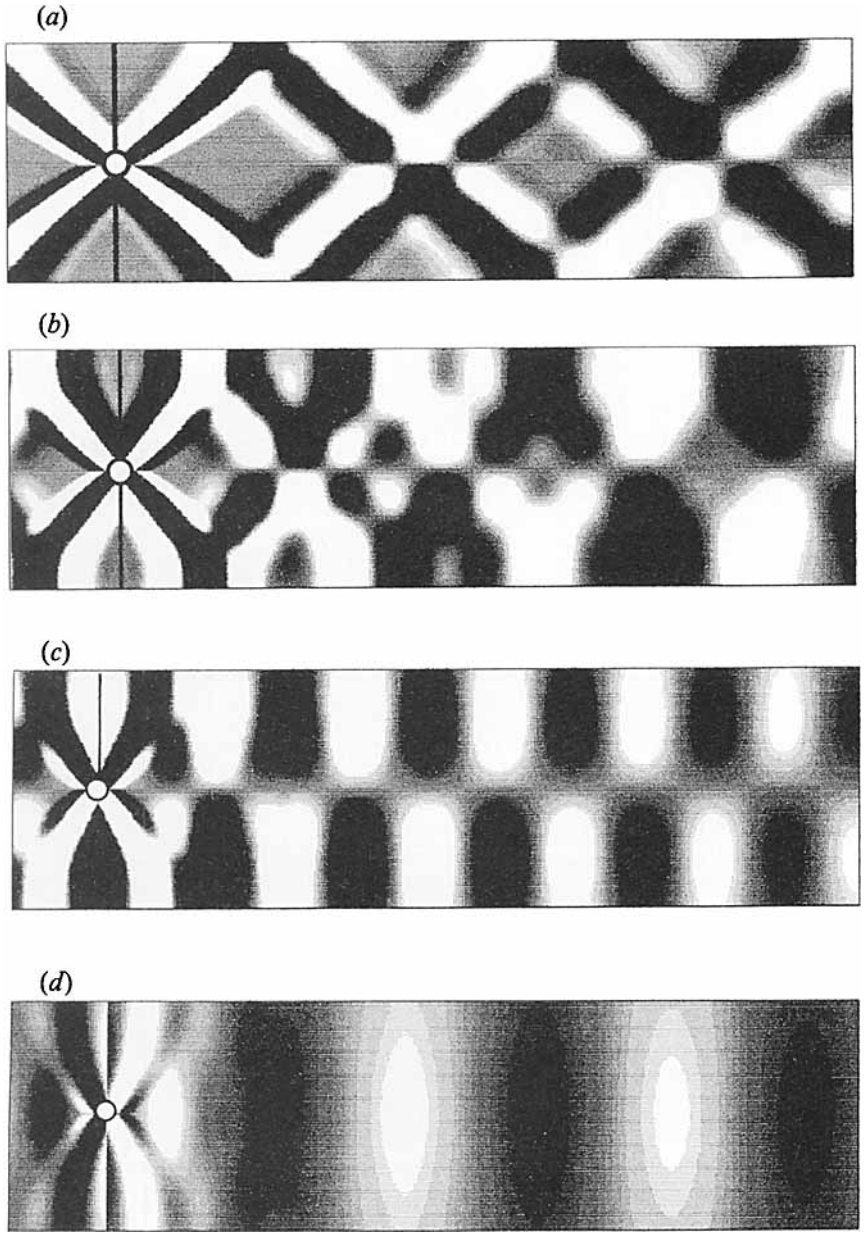

FIGURE 9. The development of thermocline waves using the simple physical model. (*a–d*) correspond to the experiments shown in figures 2(*a*)–2(*c*) and 4(*b*) respectively.

Comparing this with (11) gives

$$\Lambda_T = \frac{4X_c}{2n+1}. \tag{16}$$

Thus the number of complete wavelengths within a distance $4X_c$ is $(2n+1)$ and for the lowest mode, $n = 0$, there are four reflections of a ray path within a wavelength.

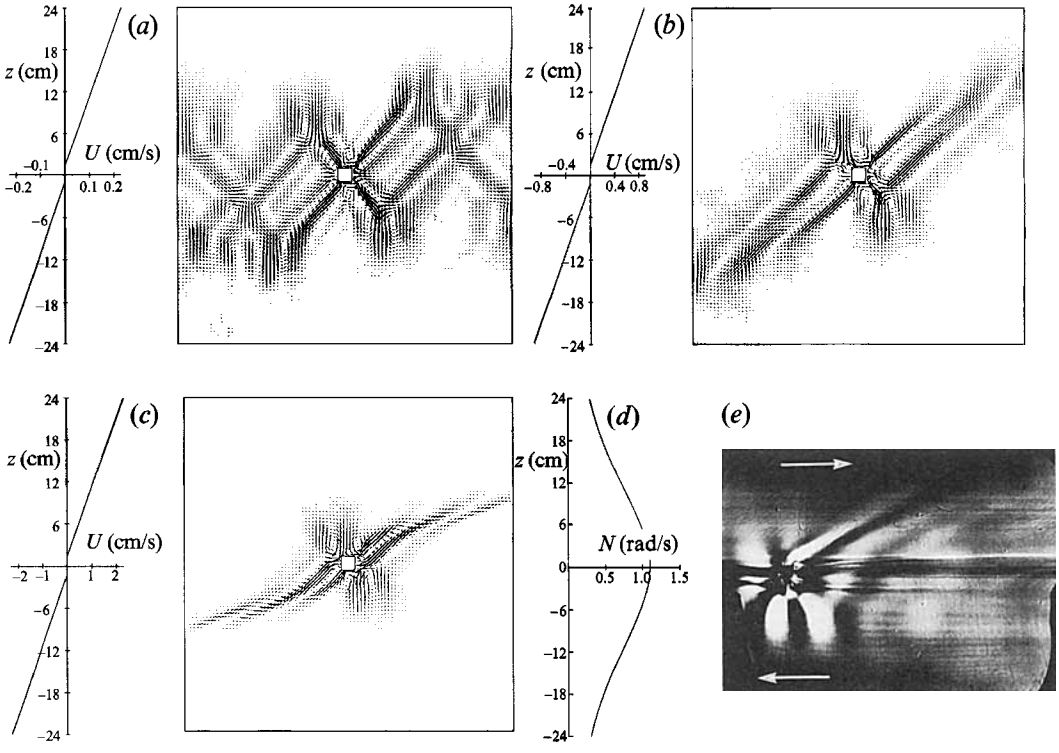

FIGURE 10. Finite-difference computations showing how the waves in a thermocline are modified when there is a shear flow, $U(z)$, with a constant velocity gradient s. $N_0 = 1.1$ rad/s, $\epsilon = 240$ mm and $\Omega = 0.67$. (*a*), (*b*) and (*c*) The velocity vector plots and the corresponding shear profiles with $s = 0.01$, 0.04 and 0.1 s^{-1} respectively. (*d*) The sech natural frequency distribution (which is the same for all the diagrams in this figure). (*e*) Schlieren photograph with conditions similar to (*c*) (MacIver 1988).

5. Waves in a thermocline with a linear shear

The way in which internal waves behave in a linear shear flow when the background natural frequency is constant was studied by Liu *et al.* (1990). It was shown that the isophase lines and the ray paths are not coincident as they are for an oscillatory disturbance in a quiescent stratified fluid. This section considers the way in which shear modifies the waves from an oscillatory source in a thermocline.

To show how shear modifies the wave pattern three examples are given in figure 10 with all parameters constant except for the shear velocity gradient. The perturbation velocity vector plots are from the finite-difference calculations. There is no initial background flow at the level of the body so that a steady wave system will not be superimposed on the oscillatory system. Above and below the body the background flow has initially a constant gradient, $s = \mathrm{d}U(z)/\mathrm{d}z$. The initial velocity profile is modified during the computation by the oscillating cylinder's upstream and downstream wakes and by the exchange of energy between the waves and the background flow (see Bretherton 1966; Koop & McGee 1986). Figures 10(*a*)–10(*c*) show how the waves are modified with increasing velocity gradient s, and figure 10(*e*) shows a schlieren photograph with conditions which correspond to figure 10(*c*). The shear has modified the wave patterns considerably and for the higher values of s has limited the extent to which thermocline waves develop.

Figure 11 shows ray paths and constant phase lines from the theory of §2 over a

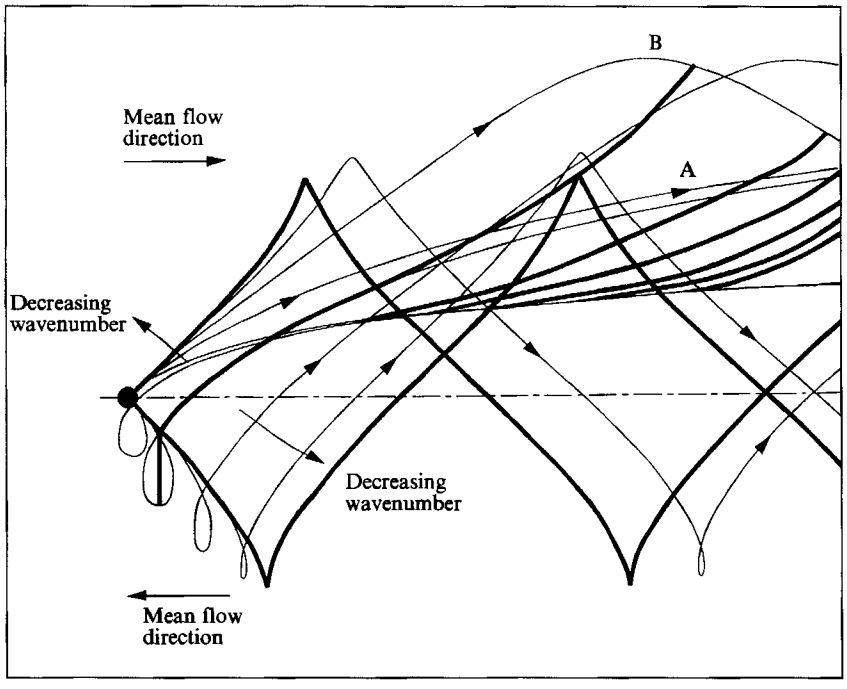

FIGURE 11. Isophase lines (——) and ray paths (——). The conditions are the same as those in figures 10(*c*) and 10(*e*) with a range of wavenumbers from 0.1 to 300 m^{-1}. The phase shift at a reflection is not included.

much wider range of wavenumbers than appear in figure 10(*c*). As the wavenumber approaches zero, the ray lines and the isophase lines become coincident, the shear having no effect. The higher wavenumbers travelling with the flow (A in figure 11) tend towards a critical level where they are absorbed by the mean flow (Koop & McGee 1986). The lower wavenumbers (B) however continually reflect at the caustics with the lowest wavenumbers reflecting at a lower level. The energy propagating against the background flow reflects back towards the centre of the thermocline, the lowest wave numbers travelling the furthest distance before reflection.

These features and the influence of the $N(z)$ and $U(z)$ distributions on energy propagation will now be analysed. From (1) and (2)

$$\sin\theta(z) = \{\omega - kU(z)\}/N(z). \tag{17}$$

Considering the solution for $\omega_r \geqslant 0$, because $\omega_r < 0$ gives a duplicate solution, and using $U(z) = sz$ then (17) becomes

$$\operatorname{sech}(Z)\,|\sin\theta(z)| = \Omega - \frac{ks\epsilon}{2N_c} Z. \tag{18}$$

Reflection occurs when $\theta \to \pm\frac{1}{2}\pi$ which gives

$$ks\epsilon/N_c = (\Omega - \operatorname{sech} Z_{ref})/\tfrac{1}{2}Z_{ref}), \tag{19}$$

and transfer of energy occurs at critical levels where $\theta(z) \to 0$ which gives

$$ks\epsilon/N_c = 2\Omega/Z_{crit}. \tag{20}$$

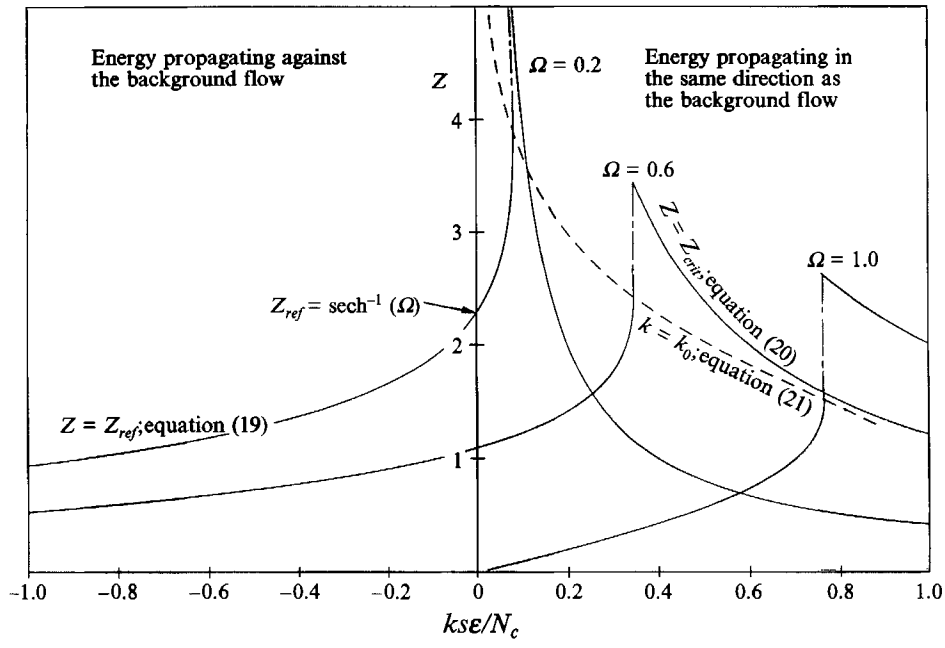

FIGURE 12. The height at which the energy of a particular wavenumber reaches either a critical level or reflects back towards the centre of the thermocline. The dashed line separates the low wavenumbers which reflect from the higher ones which reach a critical level.

Z_{ref} and Z_{crit} are the levels where either reflection or absorption occurs for the wavenumber under consideration. The curves for three different values of Ω are shown in figure 12. For energy travelling in the same direction as the background shear flow the shear and the natural frequency have opposite effects on the ray paths. The natural frequency tends to bend the ray paths towards the vertical while the shear tends to bend the rays towards the horizontal. For fixed Ω, there exists a wavenumber, k_0 say, such that energy with wavenumber $k > k_0$ will be absorbed and with $k \leqslant k_0$ will be reflected. The wavenumber k_0 can be determined by differentiating (19) with respect to Z_{ref} and equating $\mathrm{d}k/\mathrm{d}Z_{ref}$ to zero so that

$$\frac{k_0 s\epsilon}{N_c} = 2 \operatorname{sech} Z_{ref} \tanh Z_{ref}. \tag{21}$$

The curve from this equation is shown as the dashed line in figure 12 and represents the upper limit for the wavenumber beyond which energy is absorbed rather than reflected. Along the vertical axis where $ks\epsilon/N_c = 0$ the crossings of the caustic curves (19) occur at $Z_{ref} = \operatorname{sech}^{-1}(\Omega)$ and correspond to the caustics in an unsheared thermocline. $ks\epsilon/N_c \to \pm\infty$ corresponds to a sheared fluid with constant natural frequency.

Energy which is propagating against the background flow has both the natural frequency distribution and the shear acting to bend the rays towards the vertical. The energy will therefore reflect at a shorter distance from the body than would be the case if shear were not present. Once reflected, the energy will pass the level of the body and behave like the energy of the same wavenumber which propagated away from the body in the direction of the background shear flow.

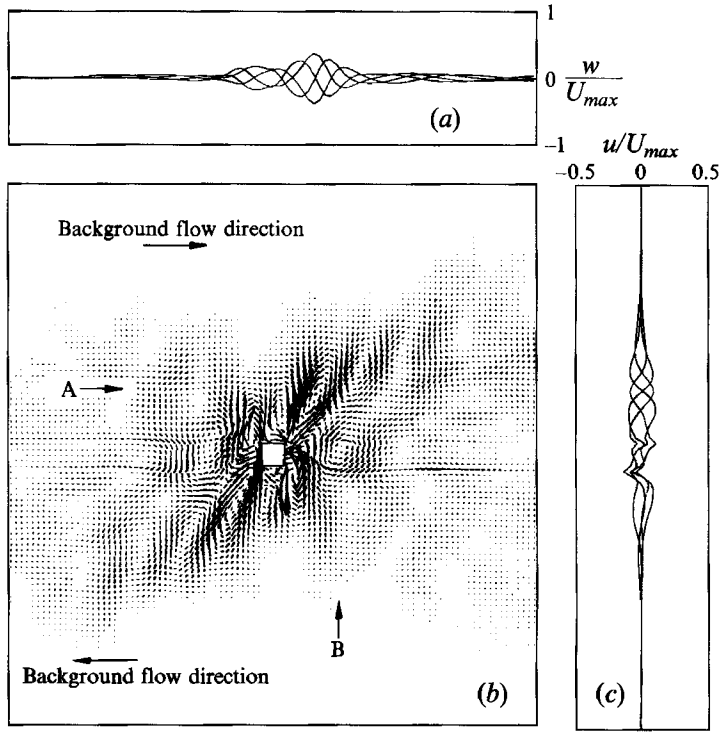

FIGURE 13. A horizontally oscillating body in a thermocline with $N_c = 1.1$ rad/s, $\epsilon = 240$ mm and $\Omega = 0.9$, as in figure 5, but now in a shear flow with $s = 0.1$ s^{-1}. (*a*) Vertical velocity distribution at level A during an oscillation period. (*b*) Velocity vector diagram. (*c*) Distribution of the horizontal velocity perturbation across the vertical plane at B.

The effect of shear on the cellular thermocline waves of figure 5 is shown in figure 13(*b*). Distorted mode $n = 1$ cells are visible near the body but decay rapidly away from the body as a result of energy being lost to the mean flow. Some perturbation velocity distributions during one oscillation period are shown in figures 13(*a*) and 13(*c*). The horizontal velocity perturbation is the difference between the velocity distribution during the oscillation and the original background flow at the beginning of the computation which is the same as that in figure 10(*c*). The 'kinks' in the horizontal velocity perturbations along horizontal lines at the top and bottom of the cylinder correspond to the difference between this initial profile and the smoothed profile which develops after the start.

6. Conclusions

Internal waves generated by an oscillating body in a thermocline have been studied experimentally, theoretically and numerically. Linear theory under the WKB approximation was shown to give a good representation of the wave patterns when the wavelength is small compared to the thickness of the thermocline. A simple physical model of widening and superimposing wave beams in a thermocline has reproduced the main features of the transition to thermocline waves. It was shown how the transition proceeds from high-mode oscillations through to the lowest odd or even mode depending on the direction of the body oscillation. The transition from a trapped cross-

wave into the mode thermocline oscillation occurs over a shorter distance as λ/ϵ increases. The presence of shear flows can inhibit the development of thermocline waves because wave energy is absorbed into the background flow near critical levels.

The work was supported by the Procurement Executive, Ministry of Defence.

REFERENCES

APPLEBY, J. C. & CRIGHTON, D. G. 1986 Non Boussinesq effects in the diffraction of internal waves from an oscillating cylinder. *Q. J. Mech. Appl. Maths* **39**, 209.

BRETHERTON, F. P. 1966 The propagation of groups of internal waves in a shear flow. *Q. J. R. Met. Soc.* **92**, 466.

GORDON, D., KLEMENT, U. R. & STEVENSON, T. N. 1975 A viscous internal wave in a stratified fluid whose buoyancy frequency varies with altitude. *J. Fluid Mech.* **69**, 615.

GROEN, P. 1948 Contributions to the theory of internal waves. *Konin. Neder. Met. Inst. Bilt. Med-en-Verhand.* Ser. B2(11).

HARLOW, F. H. & WELCH, J. E. 1965 Numerical calculation of time-dependent viscous incompressible flow of fluid with a free surface. *Phys. Fluids* **8**, 2182.

KANELLOPULOS, D. 1982 Internal wave experiments. PhD thesis, University of Manchester.

KISTOVICH, A. V., NEKLYUDOV, V. I. & CHASHECHKIN, Y. D. 1990 Non-linear two-dimensional internal waves generated by a periodically moving source in an exponentially stratified medium. *Izv. Atmos. Ocean. Phys.* **26**, No. 10.

KOOP, C. G. & MCGEE, B. 1986 Measurements of internal gravity waves in a continuously stratified shear flow. *J. Fluid Mech.* **172**, 453.

KRAUSS, W. 1966 Methoden und Ergebnisse der Theoretischen Ozeanographie. *Interne Wellen* **2**, 32.

LAWS, P., PEAT, K. & STEVENSON, T. N. 1982 An interferometer to study density stratified flows. *J. Phys.* E: *Sci. Instrum.* **15**, 1327.

LIGHTHILL, M. J. 1978 *Waves in Fluids.* Cambridge University Press.

LIU, R. 1989 A numerical and analytical study of internal waves in stratified fluids. PhD thesis, University of Manchester.

LIU, R., NICOLAOU, D. & STEVENSON, T. N. 1990 Waves from an oscillatory disturbance in a stratified shear flow. *J. Fluid Mech.* **219**, 609.

LIU, R. & STEVENSON, T. N. 1989 A finite difference method for modelling internal waves. *Aero. Rep.* 8908, Dept. of Engng, University of Manchester.

MACIVER, R. D. 1988 Experimental investigation of the interaction of internal gravity waves in a thermocline with a linear shear flow. MSc thesis, University of Manchester.

MAKAROV, S. A., NEKLYUDOV, V. I. & CHASHECHKIN, Y. D. 1990 Spatial structure of two-dimensional monochromatic internal wave beams in an exponentially stratified fluid. *Izv. Atmos. Ocean. Phys.* **26**, No. 7.

NICOLAOU, D. 1987 Internal waves around a moving body. PhD thesis, University of Manchester.

PHILLIPS, O. M. 1966 *The Dynamics of the Upper Ocean.* Cambridge University Press.

ROBERTS, J. 1975 *Internal Gravity Waves in the Ocean.* Marcel Dekker.

STEVENSON, T. N. 1973 The phase configuration of internal waves around a body moving in a density stratified fluid. *J. Fluid Mech.* **60**, 759.

STEVENSON, T. N., KANELLOPULOS, D. & CONSTANTINIDES, M. 1986 The phase configuration of trapped internal waves from a body moving in a thermocline. *Appl. Sci. Res.* **43**, 91.

THOMAS, N. H. & STEVENSON, T. N. 1972 A similarity solution for viscous internal waves. *J. Fluid Mech.* **54**, 495.

THORPE, S. A. 1968 On the shape of progressive internal waves. *Phil. Trans. Roy. Soc. Lond.* A **263**, 563.

VOISIN, B. 1991 Internal wave generation in uniformly stratified fluids. Part 1. Green's function and point sources. *J. Fluid Mech.* **231**, 439.

YOUNG, J. A. & HIRT, C. W. 1972 Numerical calculation of internal wave motions. *J. Fluid Mech.* **56**, 265.